# Synthesis and characterization of recombinant factor VIIa-conjugated magnetic iron oxide nanoparticles for hemophilia treatment

**ARTICLE** *in* JOURNAL OF BIOMEDICAL MATERIALS RESEARCH PART A · DECEMBER 2009

Impact Factor: 3.37 · DOI: 10.1002/jbm.a.32296 · Source: PubMed



**3 AUTHORS**, INCLUDING:

Gilead Shafir
Bar Ilan University
**3** PUBLICATIONS **68** CITATIONS

SEE PROFILE

Anna Galperin
University of Washington Seattle
**16** PUBLICATIONS **252** CITATIONS

SEE PROFILE

# Synthesis and characterization of recombinant factor VIIa-conjugated magnetic iron oxide nanoparticles for hemophilia treatment

**Gilead Shafir,* Anna Galperin,* Shlomo Margel**
*Department of Chemistry, Bar-Ilan University, Ramat-Gan 52900, Israel*

Received 30 December 2007; revised 10 June 2008; accepted 25 August 2008
Published online 23 December 2008 in Wiley InterScience (www.interscience.wiley.com). DOI: 10.1002/jbm.a.32296

**Abstract:** Maghemite ($\gamma$-$Fe_2O_3$) nanoparticles of 15.0 $\pm$ 2.1 nm in diameter were prepared by nucleation, followed by controlled growth of magnetic iron oxide thin films onto gelatin nuclei. Functionalization of these magnetic nanoparticles with activated double bonds was accomplished by interacting divinyl sulfone with the gelatin coating of the $\gamma$-$Fe_2O_3$ nanoparticles. The activated double bonds were then used for covalent binding, via Michael addition reaction, of recombinant factor VIIa and human serum albumin to the surface of these nanoparticles. Recombinant factor VIIa was also physically bound to the magnetic nanoparticles by interacting this factor with the human serum albumin conjugated $\gamma$-$Fe_2O_3$ nanoparticles. The influence of factor VIIa concentration on the immobilization yield has been elucidated. Leakage of the bound factor VIIa into PBS containing 4% albumin was insignificant. The coagulant activity of the physically adsorbed recombinant factor VIIa was similar to that of the free one and was significantly better than that of the covalently bound. The blood half-life of free factor VIIa is short, about 2–3 h, because of digestion by proteolytic enzymes and inhibitory effects. Stabilization of factor VIIa against trypsin (a model proteolytic enzyme) and chloromethyl ketone-type inhibitor was accomplished by conjugation of the factor to the $\gamma$-$Fe_2O_3$ nanoparticles. This stabilization may extend the blood half-life of factor VIIa. Therefore, IV injection of factor VIIa conjugated $\gamma$-$Fe_2O_3$ nanoparticles instead of free factor may avoid the frequent dosing and reduce the cost of hemophilia treatment. © 2008 Wiley Periodicals, Inc. J Biomed Mater Res 91A: 1056–1064, 2009

**Key words:** iron oxide nanoparticles; factor VIIa; surface modification; biofunctionalization; hemophilia

## INTRODUCTION

Hemostasis is the body's normal physiological response for arresting of hemorrhage following vascular injury. Blood coagulation is one of the major pathophysiological mechanisms involved in hemostasis whereby a damaged blood vessel wall is covered by a fibrin clot to stop hemorrhage and aid repair of the damaged vessel. The currently accepted model of blood coagulation involves a cascade of clotting factors activation reactions that follows one of two separate pathways, termed intrinsic and extrinsic, which converge to a common pathway.[1,2] The common pathway leads to clot formation through conversion of the soluble protein fibrinogen to insoluble cross-linked fibrin, by the clotting factor thrombin.[1]

Factor VIIa (FVIIa), a two chain peptide, is one of several clotting factors involved in the blood coagulation cascade. FVIIa plays a key role in the initiation of the extrinsic pathway through binding to the integral membrane glycoprotein, tissue factor (TF). This TF/FVIIa enzymatically active complex then activates the factors IX and X and, ultimately, leads to thrombin generation and clot formation.[3–5]

Genetic and acquired deficiencies in the clotting proteins factor VIII (FVIII) and factor IX (FIX), which participate in the intrinsic pathway of the coagulation cascade, lead to the most common bleeding disorders, hemophilia A and hemophilia B, respectively.[6–8] At present, hemophilia treatment is mainly done by IV administration of human plasma-derived monoclonal antibody-purified FVIII and FIX concentrates and recombinant FVIII and FIX.[8]

Approximately 10–20% of patients with hemophilia A and 3% of patients with hemophilia B develop inhibitory antibodies against the added factors

*These authors contributed equally to this work.

*Correspondence to:* S. Margel; e-mail: shlomo.margel@mail.biu.ac.il

Contract grant sponsors: The Israeli Ministry of Commerce and Industry, Rad Biomed Incubator Ltd.

VIII or IX.[9–12] As a result, the added factors are neutralized, the bleeding does not stop, and an alternative treatment needs to be considered. During the past decade, recombinant FVIIa (rFVIIa) has been used successfully for hemophilia treatment in patients with and without inhibitory antibodies, especially those undergoing surgical procedures.[2,13] The mechanism by which high doses of FVIIa restore normal hemostasis in the hemophilia situation is not clear, although it has been hypothesized that FVIIa is able to trigger sufficient thrombin generation in hemophilia blood.[2] rFVIIa has also been suggested for treatment of bleeding associated with trauma and surgery in patients without coagulation defects.[2,14,15]

The main disadvantage of FVIIa is its short half-life *in vivo*, about 2–3 h, compared with ~12 and 24 h for FVII and FIX, respectively.[13,16,17] It requires, therefore, frequent IV injections of the factor in order to maintain hemostasis, which cause this treatment to be very expensive.[16,18,19] For example, the cost of a single average 90 μg/kg dose of rFVIIa to a 80-kg person is about US$4500, while the dosing ranges from 90 to 300 μg/kg.

This article describes a method to stabilize FVIIa by immobilizing this factor to γ-$Fe_2O_3$ magnetic nanoparticles.[20–23] Magnetic iron oxide nanoparticles are biodegradable and nontoxic and are widely investigated for various biomedical applications.[24–37]

The maghemite nanoparticles described in this article have been prepared by nucleation, followed by controlled growth of magnetic iron oxide thin films onto gelatin nuclei, according to Margel and Gura.[35] Functionalization of these iron oxide nanoparticles with activated double bonds was accomplished by interacting divinyl sulfone (DVS) with the gelatin coating of these magnetic nanoparticles. Residual activated double bonds were then used for covalent binding, via Michael addition reaction, of rFVIIa and human serum albumin (HSA) to the surface of the γ-$Fe_2O_3$ nanoparticles. rFVIIa was also physically attached to the magnetic nanoparticles by interacting the factor with the HSA-conjugated nanoparticles. The coagulant activity of the physically adsorbed rFVIIa was similar to that of the free one and significantly better than that of the covalently bound one. Leakage of the conjugated FVIIa into PBS containing 4% albumin was insignificant. Stabilization of FVIIa against a model of a proteolytic enzyme and a chloromethylketone (CMK)-type inhibitor was demonstrated by conjugation of the factor to the γ-$Fe_2O_3$ nanoparticles. This stabilization may extend the blood half-life of FVIIa. Therefore, IV injection of rFVIIa γ-$Fe_2O_3$-conjugated nanoparticles instead of free factor may avoid the frequent dosing of this factor and reduce the cost of the hemophilia treatment by reducing the amount of drug used.

## EXPERIMENTAL

### Materials

The following analytical-grade chemicals and kits were purchased from commercial sources and were used without further purification: ferric chloride tetrahydrate, sodium hydroxide (standard solution 1*M*), sodium bicarbonate, triethyl amine (TEA), sodium nitrite, DVS, gelatin from porcine skin, and HSA (99%) from Sigma; rFVIIa from Novo Nordisk Pharmaceuticals, Denmark; methoxy polyethylene (PEG) amine (MW 5.000) from Shearwater Polymers, USA; phosphate-buffered saline (PBS) tablets from Dulbecco A, Oxoid, England; PPA-CMK from Calbiochem, USA; ELIZA kit for FVII determination (ASSERACHROM® VII:Ag) from Diagnostica Stago, France; FVII-deficient plasma from Diagnostica Stago, France; NEOPLASTINE® Cl PLUS kit for PT determination from Diagnostica Stago; reverse cellulose membranes (MWCO12–14.000) from Spectrum, USA; MACS separation columns from Almog Diagnostic, Israel. Water was purified by passing deionized water through an Elgastat Spectrum reverse osmosis system (Elga, High Wycombe, UK).

### Synthesis of γ-$Fe_2O_3$ nanoparticles

γ-$Fe_2O_3$ magnetic nanoparticles with average diameter of about 15.0 ± 2.1 nm (as measured by TEM) were prepared by nucleation, followed by controlled growth of magnetic iron oxide thin films onto gelatin nuclei, according to Margel and Gura.[35] Briefly, 240 mg of gelatin was dissolved in 80 mL of water at 60°C. Then, 160 μL of $Fe^{+2}$ solution (10 mmol in 5 mL 0.1*N* HCl) and 57.6 μL of sodium nitrite solution (7.27 mmol in 5 mL $H_2O$) were added to the shaken gelatine solution. For nucleation, titration with sodium hydroxide (1*M*) was then performed until a pH of 9.5 was reached. This procedure was repeated successively four more times. Then, the reaction mixture was shaken at 60°C for an additional 1 h. The obtained γ-$Fe_2O_3$ nanoparticles were washed from nonmagnetic waste using the high-gradient magnetic field (HGMF) technique.[35] For a detailed description of the HGMF technique, see Ref. 37.

### Synthesis of DVS-derivatized γ-$Fe_2O_3$ nanoparticles

DVS (2.4 mL) was added to 200 mL aqueous dispersion of γ-$Fe_2O_3$ nanoparticles (3 mg/mL). TEA was then gradually added until a pH of 10.5 was reached. The reaction mixture was then shaken at 60°C for 18 h. The obtained DVS derivatized magnetic iron oxide nanoparticles were then washed free from nonmagnetic waste using the HGMF technique.

### Covalent conjugation of rFVIIa to the DVS-derivatized γ-$Fe_2O_3$ nanoparticles

γ-$Fe_2O_3$-FVIIa nanoparticles were synthesized by adding 200 μL of rFVIIa aqueous solution (0.6 mg/mL) to 600 μL

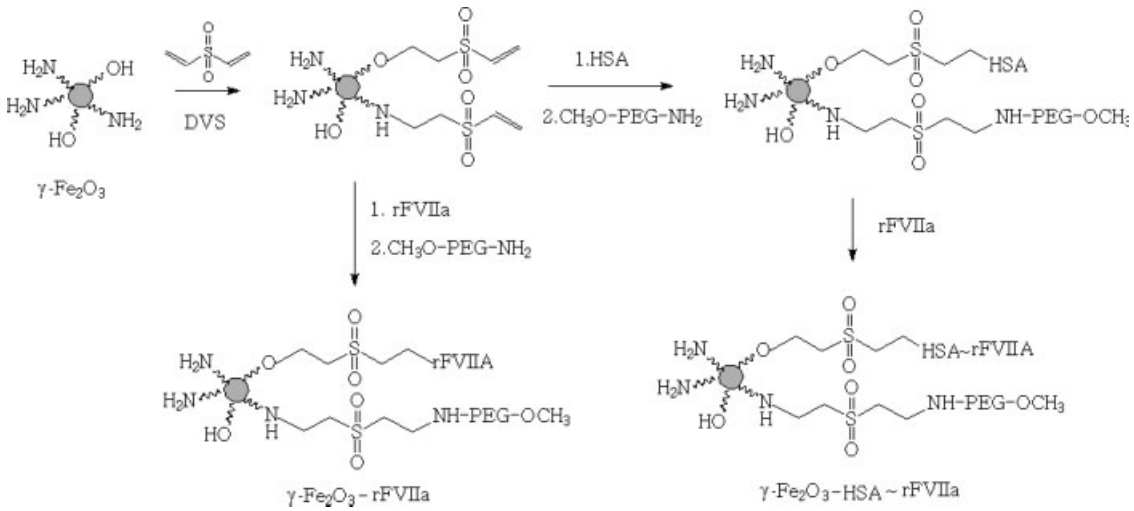


**Figure 1.** Covalent and physical conjugation of rFVIIa to the $\gamma$-$Fe_2O_3$ nanoparticles. "-" and "$\sim$" are symbols for the covalent and physical attachment, respectively, of the rFVIIa to the $\gamma$-$Fe_2O_3$ nanoparticles.

of DVS-derivatized $\gamma$-$Fe_2O_3$ nanoparticles dispersed in bicarbonate-buffered solution (2 mg/mL, pH 8.4) ([nanoparticles]/[rFVIIa] = 10 w/w). The reaction mixture was then shaken at room temperature for 18 h. Then, residual activated double bonds of the DVS-derivatized magnetic nanoparticles were blocked by the addition of methoxy-PEG-amine (1%, w/v). The mixture was then shaken for additional 2 h. The obtained $\gamma$-$Fe_2O_3$-FVIIa nanoparticles were then washed from nonmagnetic waste using the HGMF technique. A similar experiment was also performed using a weight ratio [nanoparticles]/[rFVIIa] of 50, substituting the 200 μL of the rFVIIa aqueous solution for 40 μL.

## Physical conjugation of rFVIIa to the $\gamma$-$Fe_2O_3$ nanoparticles

Physical conjugation of the rFVIIa to the $\gamma$-$Fe_2O_3$ nanoparticles was performed through two respective steps, as shown in Figure 1. In the first step (A), HSA coating on the $\gamma$-$Fe_2O_3$ nanoparticles was performed. This step was accomplished by the covalent binding of HSA to the DVS-derivatized $\gamma$-$Fe_2O_3$ nanoparticles, via Michael addition reaction. In the second step (B), physical conjugation of the rFVIIa to the $\gamma$-$Fe_2O_3$ nanoparticles via its HSA coating was accomplished. A detailed procedure is described below.

### A. Covalent conjugation of HSA to the DVS-derivatized $\gamma$-$Fe_2O_3$ nanoparticles

Two hundred fifty milligrams of HSA was added to 100 mL of DVS-derivatized $\gamma$-$Fe_2O_3$ nanoparticles dispersed in bicarbonate buffer (2.5 mg/mL, pH 8.4). The reaction mixture was then shaken at room temperature for 24 h. Then, residual activated double bonds of the DVS-derivatized magnetic nanoparticles were blocked by addition of methoxy-PEG-amine (1%, w/v). The mixture was then shaken for additional 2 h. The obtained $\gamma$-$Fe_2O_3$-HSA nanoparticles were then washed from nonmagnetic waste using the HGMF technique.

### B. Physical attachment of rFVIIa to the $\gamma$-$Fe_2O_3$-HSA nanoparticles

Two hundred microliters of rFVIIa aqueous solution (0.6 mg/mL) were added to 600 μL of $\gamma$-$Fe_2O_3$-HSA nanoparticles dispersed in a PBS solution (2 mg/mL, pH = 7.3) ([nanoparticles]/[rFVIIa] = 10 w/w). The reaction mixture was then shaken at room temperature for 18 h. The obtained $\gamma$-$Fe_2O_3$-HSA$\sim$rFVIIa nanoparticles were washed from nonmagnetic waste using the HGMF technique. A similar experiment was also performed using a weight ratio [nanoparticles]/[rFVIIa] of 50, by substituting the 200 μL of the rFVIIa aqueous solution for 40 μL.

## Binding yield and bound concentration of rFVIIa to the magnetic nanoparticles

The concentration of rFVIIa bound to the magnetic nanoparticles was determined by measuring the unbound rFVIIa with the ELIZA kit (ASSERACHROM VII:Ag) and subtracting it from the initial concentration. The binding yield was calculated by multiplying the ratio between the concentration of the bound factor and the initial concentration by 100.

## rFVIIa leakage extent

The leakage of rFVIIa, bonded covalently or physically to the $\gamma$-$Fe_2O_3$ nanoparticles, into PBS containing 4% HSA was evaluated using the following procedure.

$\gamma$-$Fe_2O_3$-rFVIIa or $\gamma$-$Fe_2O_3$-HSA$\sim$rFVIIa nanoparticles dispersed in a PBS buffer containing 4% HSA (2.5 mg/mL, pH 7.3) were shaken at room temperature for about 24 h.

Then, the FVIIa-conjugated nanoparticles were extracted from the supernatant using the HGMF technique and the concentration of rFVIIa in the filtrate was determined by the ELIZA kit (ASSERACHROM VII:Ag).

### Coagulant activity of free and bound rFVIIa

The clotting time of deficient FVII plasma treated by free or bound rFVIIa was determined using the PT test with the STart-4 analyzer according to the following procedure: 10 μL of free/conjugated rFVIIa in PBS (0.01 mg/mL) were added to 90 μL of deficient FVII plasma. The mixture was then incubated for 1 min at 37°C. Then, 100 μL of thromboplastine aqueous solution (taken from the NEOPLASTINE® Cl PLUS kit) was added and the PT value of the plasma was measured. Each reported PT value is an average of three triplicate measurements.

### Effect of trypsin on the coagulant activity of free and conjugated rFVIIa

Ten micrograms of trypsin was added to 1000 μL of free/conjugated rFVIIa in PBS 0.01 mg/mL ([trypsin]/[rFVIIa] = 1 w/w). The mixture was then incubated at room temperature for different time periods. At each period of time the PT value of the deficient FVIIa plasma was measured. Each reported PT value is an average of three triplicate measurements. The trypsin effect on the PT of the plasma was studied at different [trypsin]/[rFVIIa] weight ratios.

### Effect of PPA-CMK on the coagulant activity of free and conjugated rFVIIa

0.1 μL of PPA-CMK (50 mg/mL) was added to 500 μL of free/conjugated rFVIIa in PBS (0.01 mg/mL, [PPA-CMK]/[rFVIIa] = 1 w/w). The mixture was then incubated at room temperature for 18 h. Then, the PPA-CMK-treated free/conjugated rFVIIa was washed from excess reagents using intensive dialysis cycles in PBS at 4°C. The PT value of the deficient FVIIa plasma was then measured. Each reported PT time is an average of three triplicate measurements. The inhibition effect on the PT was also studied at different [PPA-CMK]/[rFVIIa] weight ratios.

### Characterization

TEM pictures were obtained with a JEOL-JEM 100SX electron microscope with 80–100 kV of accelerating voltage. Samples for TEM were prepared by placing a drop of diluted sample on a 400-mesh carbon-coated copper grid. The dry particles' average size and distribution were determined by measuring the diameter of more than 100 particles with the image analysis software AnalySIS Auto (Soft Imaging System GmbH, Germany).

The hydrodynamic diameter and size distribution of the nanoparticles dispersed in aqueous phase were determined using a submicron particle analyzer, model N4 Plus (Coulter Electronics, England).

Magnetic measurements were performed at room temperature using an Oxford Instrument vibrating sample magnetometer.

The PT test was performed with the STart-4 analyzer (Diagnostica Stago, France).

## RESULTS AND DISCUSSION

$\gamma$-$Fe_2O_3$ nanoparticles of 15.0 ± 2.1 nm of average diameter were prepared by nucleation, followed by controlled growth of maghemite thin films onto gelatin nuclei, according to Margel and Gura.[35] Figure 1 describes the general approach through which covalent and physical immobilization of rFVIIa onto the surface of the maghemite nanoparticles has been performed. These maghemite nanoparticles contain gelatin within and on the surface of the nanoparticles. The surface gelatin provides functional groups, for example, primary amines and hydroxyls, through which functionalization of these nanoparticles with activated double bonds was accomplished, via Michael addition interaction with excess DVS. The residual activated double bonds of the DVS-derivatized maghemite nanoparticles were then used for covalent binding, via Michael addition reaction, of rFVIIa or HSA to the surface of the $\gamma$-$Fe_2O_3$ nanoparticles. Blocking of remaining double bonds was then performed with methoxy-PEG-amine. rFVIIa was also physically attached to the magnetic nanoparticles by interacting the factor VIIa with the HSA-conjugated nanoparticles (see Fig. 1). This physical conjugation is based on the high affinity of HSA to various peptides and plasma proteins, including clotting proteins such as thrombin.[22,38–41] Therefore, we assumed that FVIIa may possess high affinity toward the HSA coating on the magnetic nanoparticles.

Figure 2(A) presents a typical TEM image of the $\gamma$-$Fe_2O_3$-HSA~rFVIIa nanoparticles. This figure demonstrates the uniformity and stability of these particles against agglomeration. Careful measurements indicate that these nanoparticles have a diameter and size distribution of 23.1 ± 4.3 nm. Light scattering measurements, shown in Figure 2(B), indicate that the diameter and size distribution of the $\gamma$-$Fe_2O_3$-HAS~rFVIIa nanoparticles are 116 ± 14 nm. The difference in the diameters measured by TEM and light scattering is due to the fact that the first method measures the dry diameter of the bioactive nanoparticles, while the second one measures the hydrodynamic diameter, which takes into account the surface adsorbed solvent molecules as well as the swelling of the particles by the solvent.[42] The dry and hydrodynamic diameters of the "naked"

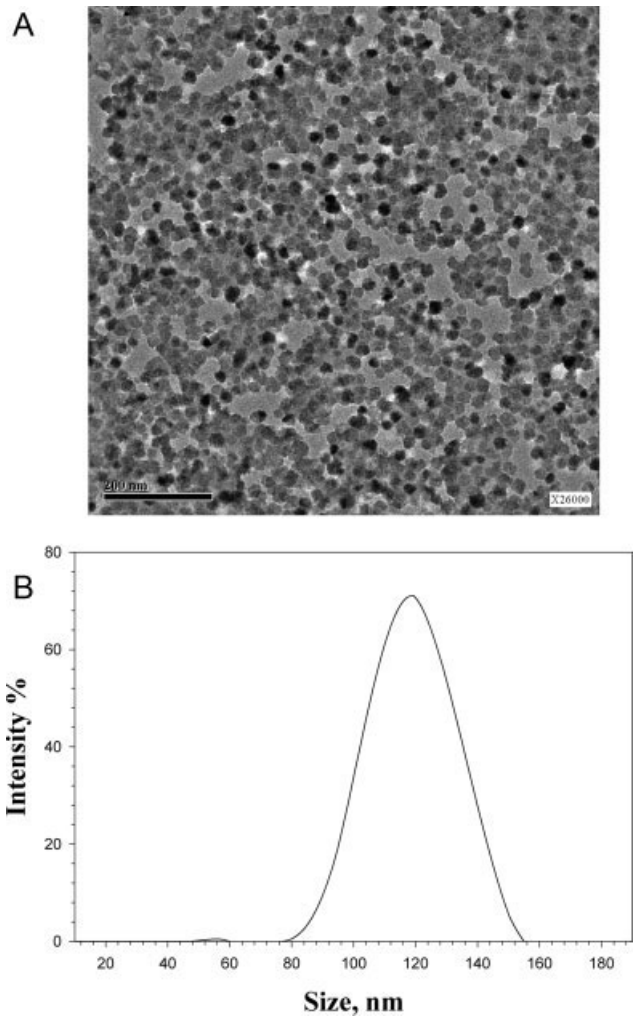


**Figure 2.** TEM image (A) and size histogram (B) of the γ-$Fe_2O_3$-HSA∼rFVIIa nanoparticles.

γ-$Fe_2O_3$ nanoparticles are 15.0 ± 2.1 and 103 ± 26 nm, respectively. The slight increase in the dry and hydrodynamic diameters of the γ-$Fe_2O_3$-HSA∼rFVIIa nanoparticles relative to the "naked" ones is probably due to the organic shell coating on the surface of the γ-$Fe_2O_3$ nanoparticles. It should be noted that the same tendency demonstrated for the physical bonded rFVIIa (γ-$Fe_2O_3$-HSA∼rFVIIa) was also observed for the covalent bonded one (γ-$Fe_2O_3$-rFVIIa), that is, these bioactive nanoparticles are uniform, stable against agglomeration, and their dry and hydrodynamic diameters are slightly higher than that of the "naked" ones.

Figure 3 demonstrates the magnetization curves of the γ-$Fe_2O_3$ (A) and the γ-$Fe_2O_3$-HSA∼rFVIIa (B) nanoparticles. These figure illustrates that the saturation magnetizations of the "naked" and the physically bonded FVIIa nanoparticles are 57 and 52 emu/g, respectively. The slight decrease in the magnetization of the FVIIa-conjugated nanoparticles is probably attributed to the organic shell coating of

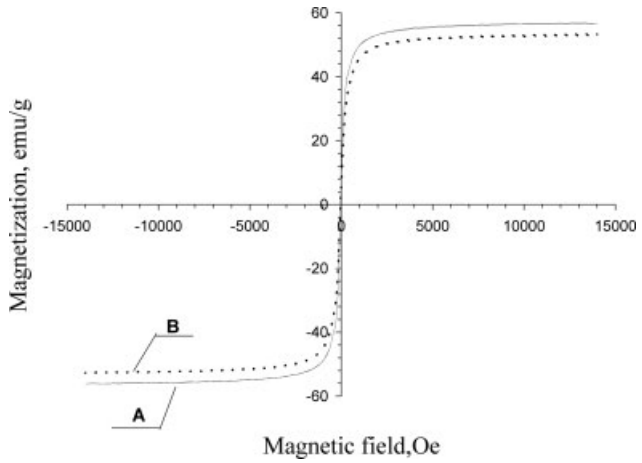


**Figure 3.** Magnetization curves at room temperature of the γ-$Fe_2O_3$ (A) and the γ-$Fe_2O_3$-HSA∼rFVIIa (B) nanoparticles.

the γ-$Fe_2O_3$ nanoparticles. The same tendency of slight decrease in saturation magnetization was also observed for the γ-$Fe_2O_3$-FVIIa nanoparticles (ca. 54 emu/g).

Table I demonstrates the immobilization yield and the concentration of the covalent and physical bound rFVIIa for [nanoparticles]/[rFVIIa] weight ratios of 10 and 50. Table I indicates that the immobilization yield of the covalent conjugation is higher than that of the physical one for both weight ratios. For example, for the weight ratio 10 the covalent and physical immobilization yield is 94 and 78%, respectively. For the weight ratio 50 the immobilization yield increased for both conjugation techniques, but still the yield of the covalent conjugation is higher than that of the physical adsorption: 97 and 88%, respectively. Table I also illustrates that for both immobilization types, the concentration of the bound FVIIa for the weight ratio 50 is lower than for 10:20 and 93 (μg rFVIIa/mg nanoparticles), respectively, for the covalent conjugation; 18 and 78 (μg rFVIIa/mg nanoparticles), respectively, for the physical adsorption. This difference in the concentration of the bound

**TABLE I**
**Influence of the Weight Ratio [Nanoparticles]/[rFVIIa] on the Conjugation Yield and the Concentration of the rFVIIa Bound to the γ-$Fe_2O_3$ Nanoparticles[a]**

| [Nanoparticles]/[rFVIIa] (w/w) | Conjugation Yield (wt %) | | [Bound rFVIIa] (μg rFVIIa/mg particles) | |
|---|---|---|---|---|
| | Covalent | Physical | Covalent | Physical |
| 10 | 94 | 78 | 93 | 78 |
| 50 | 97 | 88 | 20 | 18 |

[a]The immobilization yield and the concentration of the rFVIIa bound to the γ-$Fe_2O_3$ nanoparticles were calculated according to the description in the "Experimental" section.

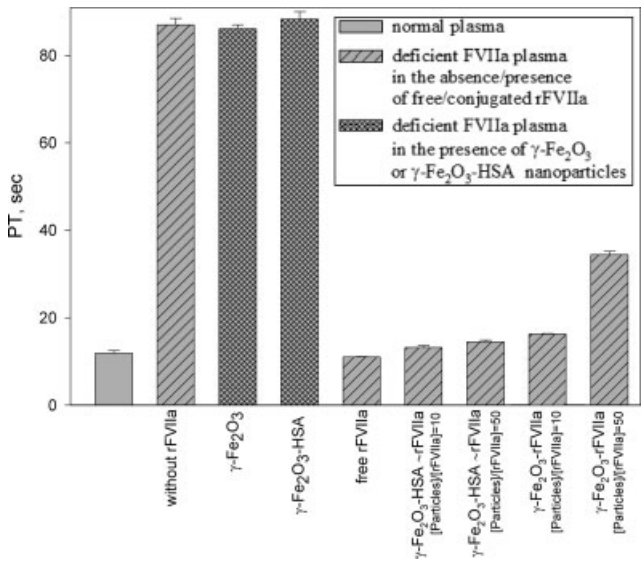


**Figure 4.** Coagulant activity of the free and the conjugated rFVIIa prepared at [Nanoparticles]/[rFVIIa] weight ratios of 10 and 50. The coagulant activity of the control nanoparticles ($\gamma$-$Fe_2O_3$ and $\gamma$-$Fe_2O_3$-HSA) and of the free/conjugated rFVIIa was evaluated by PT test performed on deficient FVII plasma according to the experimental section.

rFVIIa is reasonable, because, for the weight ratio [nanoparticles]/[rFVIIa] of 50, there is less rFVIIa than for the ratio 10.

Leakage of the covalently and physically bound rFVIIa from the surface of the $\gamma$-$Fe_2O_3$ nanoparticles into PBS containing 4% HSA was measured according to the description in the "Experimental" section. The % measured leakage at both [nanoparticles]/[rFVIIa] weight ratios of 10 and 50 was insignificant: 1% (of the bound FVIIa) for the covalently bound rFVIIa and 1.5% for the physically attached. These results indicate that indeed the coagulant activity of the bioactive nanoparticles is due to the bound FVIIa and not to the leaked FVIIa.

The coagulant activity of the conjugated rFVIIa versus the same concentration of the free one was evaluated using the prothrombin (PT) test. In general, the PT test is a basic coagulation test, useful in the assessment of congenital and/or acquired deficiencies of the extrinsic coagulation pathway, for example, the deficiency of FVII. The principle of the test consists of measuring the clotting time of the patient's plasma and comparing it with that of normal standard. In this study, the PT test was used for evaluation of the coagulant activity of the free and conjugated FVIIa by measuring the clotting time of deficient FVII plasma before and after addition of the free/conjugated rFVIIa. The PT for normal plasma of a healthy human is in the range of 11–16 s,[43] while the measured PT of deficient FVII plasma used in this study was 87.0 ± 1.5 s (Figure 4). Our aim is that the conjugated rFVIIa will reduce the PT of deficient FVII plasma to the normal range just as the free factor does. Figure 4 illustrates that the $\gamma$-$Fe_2O_3$ and the $\gamma$-$Fe_2O_3$-HSA nanoparticles do not influence significantly the PT of deficient FVII plasma, for example, 86.1 ± 0.9 and 88.3 ± 1.7 s, respectively. These results exclude the possibility that the $\gamma$-$Fe_2O_3$ nanoparticles and the HSA coating on these nanoparticles activate FX, thereby leading to decrease in PT of deficient FVII plasma. Figure 4 also shows that under the experimental conditions the free rFVIIa reduces the PT of deficient FVII plasma from 87.0 ± 1.5 to 11.0 ± 0.1 s, the physically conjugated rFVIIa, prepared at [nanoparticles]/[rFVIIa] weight ratios of 10 and 50 reduces the PT of this plasma to 13.2 ± 0.4 and 14.5 ± 0.4 s, respectively, and the covalently conjugated rFVIIa, prepared at [nanoparticles]/[rFVIIa] weight ratios of 10 and 50 reduces the PT of this plasma to 16.3 ± 0.1 and 34.4 ± 0.8 s, respectively. These results indicate that the physically conjugated rFVIIa at both [nanoparticles]/[rFVIIa] weight ratios reduces the abnormal value of deficient FVII plasma clotting time to the normal range, while the covalently conjugated rFVIIa reduces the PT of this plasma to a value above the normal range. It is possible to assume that because of the covalent conjugation, FVIIa undergoes some critical conformational changes which influences its coagulant activity significantly more than that of the physically bound factor. Based on the results shown in Figure 4, the $\gamma$-$Fe_2O_3$-HSA~rFVIIa nanoparticles obtained at a [nanoparticles]/[rFVIIa] weight ratio of 10 were selected for further study. Indeed, under these conditions the coagulant activity of the conjugated factor is just slightly lower than that of the free one, for example, clotting time of 13.2 ± 0.4 and 11.0 ± 0.1 s, respectively.

The half-life of free FVIIa in blood is short, about 2–3 h, because of the inhibitory effects and digestion by proteolytic enzymes. Previous studies have demonstrated that stabilization of peptides or proteins may be achieved by their conjugation to the surface of various nano or micrometer-sized particles.[20–23] For example, a significant stabilization of thrombin against antithrombin inhibitors and digestive enzymes has been illustrated by the conjugation of thrombin to albumin and iron oxide particles.[22] Figures 5 and 6 examine the stabilization of FVIIa by its physical conjugation to the $\gamma$-$Fe_2O_3$-HSA nanoparticles. This stabilization may extend the blood half-life of FVIIa. Therefore, IV injection of $\gamma$-$Fe_2O_3$-HSA~FVIIa nanoparticles instead of free factor may avoid the frequent dosing of this factor and reduce the cost of hemophilia treatment. Figure 5 shows the time effect of trypsin on the clotting time of deficient FVII plasma containing free or physically conjugated rFVIIa, at weight ratios [trypsin]/[rFVIIa] of 0.1 (A),

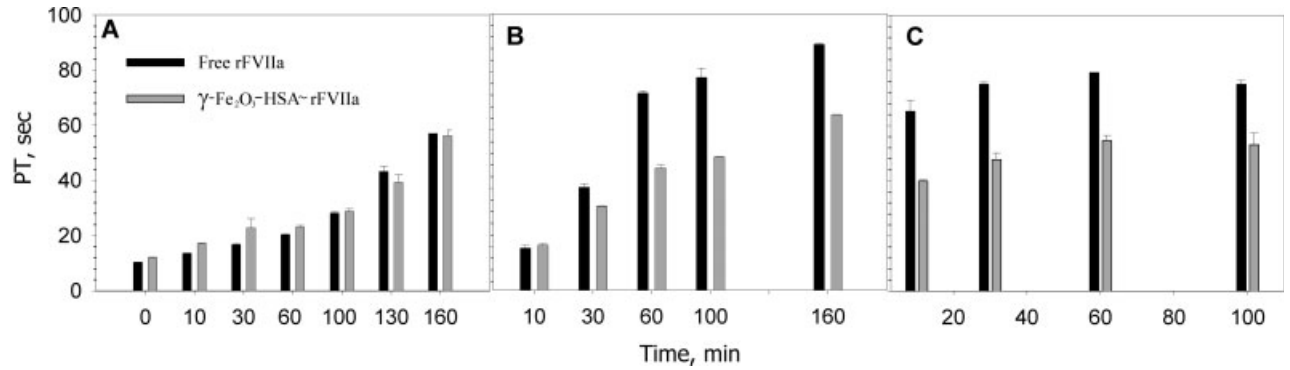


**Figure 5.** Effect of trypsin on the coagulant activity of the free/physically conjugated rFVIIa at [Trypsin]/[rFVIIa] weight ratios of 0.1 (A), 1.0 (B), and 5.0 (C). The coagulant activity of the free/conjugated rFVIIa was evaluated by PT test performed on deficient FVII plasma according to the experimental section.

1.0 (B), and 5.0 (C). This figure illustrates that the exposure to trypsin significantly decreases the coagulant activity of both the free and the conjugated factor, probably because of the digestion of the peptide by the enzyme. The damage to the coagulation activity is expressed by increasing the PT of the plasma at each time period. Figure 5 illustrates that the damage of trypsin at each specific time to the coagulant activity of the free rFVIIa is significantly higher than the damage observed for the conjugated one, and that this difference increases as the exposure time to trypsin increases. For example, Figure 5(A) illustrates that before and after exposure of the plasma to trypsin-treated free or physically conjugated rFVIIa at a weight ratio [trypsin]/[rFVIIa] of 0.1 for 100, 130, and 160 min, the measured PT values were: 10.3 ± 0.1 and 12.0 ± 0.2 sec; 28.2 ± 0.5 and 28.8 ± 0.9 sec; 43.2 ± 2.0 and 39.3 ± 2.7 sec; and 64.1 ± 1.8 and 56.2 ± 2.0 sec, respectively. These measurements indicate that before the exposure to trypsin the PT of the deficient FVIIa plasma containing the added free rFVIIa was slightly shorter than that containing the physically conjugated factor; after 100 min exposure the PT became similar, and after 130 and 160 min the opposite behavior was observed and the PT of the plasma containing the physically conjugated factor became significantly shorter than that containing the free factor. Figure 5 also illustrates that as the weight ratio [trypsin]/[rFVIIa] is increased, the rate of the damage to the coagulant activity of the free FVIIA relative to that of the physically conjugated factor increases significantly. For example, after exposure of the plasma to trypsin-treated free or physically conjugated rFVIIa at weight ratios [trypsin]/[rFVIIa] of 0.1, 1.0, and 5.0 for 10 min, the measured PT values were 13.6 ± 0.1 and 17.1 ± 0.3 sec, 19.5 ± 0.1 and 20.5 ± 0.4 sec, and 65.2 ± 4.0 and 39.9 ± 0.4 sec, respectively. Similarly, after exposure of this plasma to trypsin-treated free or physically conjugated rFVIIa for 30 min the measured PT values were 16.8 ± 0.3 and 22.8 ± 3.4 sec, 40.4 ± 1.2 and 33.9 ± 0.1 sec, and 75.0 ± 0.8 and 47.7 ± 2.4 sec, respectively. It should be emphasized that despite the fact that the PT values of the plasma after exposure to trypsin are much above the normal values, the stabilization of rFVIIa against proteolytic enzymes, for example, trypsin, by the physical conjugation of this factor to the γ-$Fe_2O_3$-HSA nanoparticles is clearly demonstrated. Regardless these encouraging results, it is clearly understood that trypsin is not a plasma protein and it serves in these studies just as a model proteolytic enzyme.

Figure 6 presents the effect of the inhibitor PPA-CMK on the PT of deficient FVIIa plasma containing

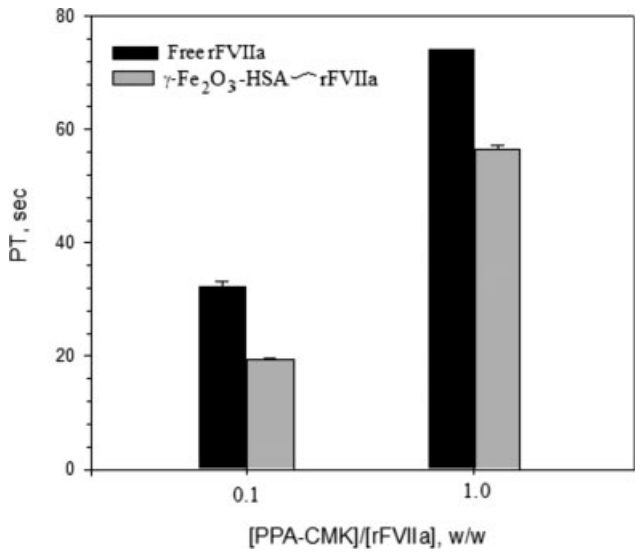


**Figure 6.** Effect of the inhibitor PPA-CMK on the coagulant activity of the free/physically conjugated rFVIIa at [PPA-CMK]/[rFVIIa] weight ratios of 0.1 and 1.0. The coagulant activity of the free/conjugated rFVIIa was evaluated by PT test performed on deficient FVII plasma according to the experimental section.

added free or physically conjugated rFVIIa at [PPA-CMK]/[rFVIIa] weight ratios of 0.1 and 1.0. This figure illustrates, as expected, that the addition of the inhibitor to deficient FVIIa plasma decreases the coagulant activity of both the free and the physically bound FVIIa. However, the extent of the decrease in the coagulant activity of the free FVIIa is significantly higher than that observed for the physically bound enzyme. For example, at a weight ratio [PPA-CMK]/[rFVIIa] of 0.1, the PT of the deficient FVIIa plasma in the presence of the free or the conjugated rFVIIa increased from 11.0 ± 0.1 and 13.2 ± 0.4 s (Fig. 4) to 32.2 ± 1.0 and 19.3 ± 0.3 s, respectively. Similarly, at a weight ratio [rFVIIa]/ [PPA-CMK] of 1.0, the PT increased to 74.1 ± 0.1 and 56.4 ± 0.7 s, respectively. This behavior may indicate that stabilization of FVIIA against inhibitory effect could be reached by its physical conjugation to the $\gamma$-$Fe_2O_3$-HSA nanoparticles.

## SUMMARY AND FUTURE PLANS

This article describes the covalent and physical conjugation of rFVIIa to $\gamma$-$Fe_2O_3$ nanoparticles of 15.0 ± 2.1 nm in diameter. Leakage of the covalent and physically bound rFVIIa from the surface of the nanoparticles into PBS containing 4% HSA was insignificant. The coagulant activity of the physically adsorbed rFVIIa was similar to that of the free one and significantly better than that of the covalently bound. This work also demonstrated that the physical conjugation of the rFVIIa to the $\gamma$-$Fe_2O_3$ nanoparticles significantly increased its stability against proteolytic enzymes, such as trypsin, and inhibitors, such as PPA-CMK. This stabilization effect may extend the blood half-life of factor VIIa. Therefore, IV injection of factor VIIa conjugated $\gamma$-$Fe_2O_3$ nanoparticles instead of free factor may avoid the frequent dosing of this factor and reduce the cost of hemophilia treatment. In future, *in vivo* trials on model animals with hemophilia A or B, aiming to compare the coagulant activity of the free rFVIIa to that of the physically conjugated factor will be designed.

The authors thank Prof. David Varon, MD (the Head of Coagulation Unit in Hadassah Medical Center) and Drs. Idan Tamir and Shoshi Keynan from "Rad Biomed Incubator" for their suggestions.

## References

1. Butenas S, Mann KG. Blood coagulation. Biochemistry 2002;67:5–15.
2. Aitken MG. Recombinant factor VIIa. Emerg Med Australas 2004;16:446–455.
3. Jenny NS, Mann KG. Coagulation cascade: An overview. In: Loscalzo J, Schafer AI, editors. Thrombosis and Hemorrhage. Baltimore, MD: Williams and Wilkins; 1998. p 3–27.
4. Butenas S, Brummel KE, Branda RF, Paradis SG, Mann KG. Mechanism of factor VIIa-dependent coagulation in hemophilia blood. Blood 2002;99:923–930.
5. Nemerson Y. The tissue factor pathway of blood coagulation. Semin Hematol 1992;29:170–176.
6. Gistschier J, Kogan S, Diamond C, Levinson B. Genetic basis of hemophilia. Trom Haemost 1991;66:37–39.
7. McGraw RA, Davis LM, Lundblad RL, Stafford DW, Roberts HS. Structure and function of factor IX: Defects in haemophilia B. Clin Haematol 1985;14:359–383.
8. Butenas S, Brummel KE, Branda RF, Paradis SG, Mann KG. Influence of factor VIIa and phospholipids on coagulation in "acquired" hemophilia. Arterioscler Thromb Vasc Biol 2003; 23:123–129.
9. Nilsson IM, Berntorp E, Zettervall O. Induction of split tolerance and clinical cure in high-responding hemophiliacs with factor IX antibodies. Proc Natl Acad Sci USA 1986;83:9169–9173.
10. Nuss R, Jacobson L, Hathaway WE, Manco-Johnson M. Evidence for antiphospholipid antibodies in hemophilic children with factor VIII inhibitors. Recombinate PUP Study Group. Thromb Haemost 1999;82:1559–1560.
11. Parquet A, Laurian Y, Rothschild C, Navarro R, Guérois C, Gay V, Durin A, Peynet J, Sultan Y. Incidence of factor IX inhibitor development in severe haemophilia B patients treated with only one brand of high purity plasma derived factor IX concentrate. Thromb Haemost 1999;82:1247–1249.
12. Chaney JD, Nielsen VG. Considerations for the hemophiliac patient with inhibitors to factor VIII. Anesth Analg 2001; 92:785–786.
13. Abshire T Kenet G. Recombinant factor VIIa: Review of efficacy, dosing regimens and safety in patients with congenital and acquired factor VIII or IX inhibitors. J Thromb Haemost 2004;2:899–909.
14. Kenet G, Walden R, Eldad A, Martinowitz U. Treatment of traumatic bleeding with recombinant factor VIIa. Lancet 1999;354:1879–1879.
15. Goodnough LT, Shander AS. Recombinant factor VIIa: Safety and efficacy. Curr Opin Hematol 2007;14:504–509.
16. Bonde C, Jensen MB. Continuous infusion of recombinant activated factor VII: Stability in infusion pump system. Blood Coagul Fibrinolysis 1998;9:103–105.
17. Lee CA, Berntrorp EE, Hoots WK, Aledort LM, editors. Textbook of Hemophilia, Chapter 40: Gene therapy: Molecular engineering of factor VIII and factor IX. Massachusetts: Blackwell Publishing; 2005. p 229–234.
18. Levi M, Peters M. Efficacy and safety of recombinant factor VIIa for treatment of severe bleeding: A systematic review. Crit Care Med 2005;33:883–890.
19. Goudemand J. Hemophilia. Treatment of patients with inhibitors. Cost issues. Haemophilia 1999;5:397–401.
20. Green-Sadan T, Kuttner T, Lublin-Tennenbaum T, Kinor N, Boguslavsky Y, Margel S, Yiadid G. Glial cell line-derived neurotrophic factor-conjugated nanoparticles suppress acquision of cacaine self-administration in rats. Exp Neurol 2005; 194:97–105.
21. Brigger I, Dubernet C, Couvreur P. Nanoparticles in cancer therapy and diagnosis. Adv Drug Delivery Rev 2002;54:631–651.
22. Margel S, Sheichat L, Tennenbaum T. Biological glues based on thrombin conjugated nanoparticles. Patent No. PTC/IL03/00977 (2004).
23. Dordick J, Kane R, Asuri P, Karajanagi, S. Enhanced stability of proteins immobilized on nanoparticles. Patent No. PTC/US2005/031652 (2007).

24. Babes L, Denizot B, Tanguy G, Jacques J, Jenue L, Jallet P. Synthesis of iron oxide nanoparticles used as MRI contrast agents: A parametric study. J Colloid Interface Sci 1999;212: 474–482.
25. Kim DK, Zhang Y, Kehr J, Klason T, Bjelke B, Muhammed M. Characterization and MRI study of surfactant-coated superparamagnetic nanoparticles administered into rat brain. J Magn Magn Mater 2001;225:256–261.
26. Hergt R, Hiergeist R, Hilger I, Kaiser WA, Lapatnikov Y, Margel S, Richter U. Maghemite nanoparticles with very high AC-losses for application in RF-magnetic hyperthermia. J Magn Magn Mater 2003;270:345–357.
27. Pardoe H, Clark PR, St Pierre TG, Moroz P, Jones SK. A magnetic resonance imaging based method for measurement of tissue iron concentration in liver arterially embolized with ferrimagnetic particles designed for magnetic hyperthermia treatment of tumors. Mag Reson Imaging 2003;21: 483–488.
28. Chemla YR, Crossman HL, Poon Y, McDermott R, Stevens R, Alper MD, Clarke J. Ultrasensitive magnetic biosensor for homogeneous immunoassay. Proc Natl Acad Sci USA 2000;97: 14268–14272.
29. Uhlen M. Magnetic separation of DNA. Nature 1989;340:733–734.
30. Debuire B, Chabli A, Frenoy N. Fast, manual, nonradioactive method for DNA sequencing. Clin Chem 1993;39:1682–1685.
31. Yoza B, Matsumoto M, Matsunaga T. DNA extraction using modified bacterial magnetic particles in the presence of amino silane compound. J Biotechnol 2002;94:217–224.
32. Scherer F, Anton M, Schillinger U, Henke J, Bergemann C, Kruger A, Gansbacher B, Plank C. Magnetofection: Enhancing and targeting gene delivery by magnetic force in vitro and in vivo. Gene Ther 2002;9:102–109.
33. Bergemann C, Muller-Schulte D, Oster J, A Brassard L, Lubbe AS. Magnetic ion-exchange nano- and microparticles for medical, biochemical and molecular biological applications. J Magn Magn Mater 1999;194:45–52.
34. Rudge SR, Kurtz TL, Vessely CR, Catterall LG, Williamson DL. Preparation, characterization, and performance of magnetic iron-carbon composite microparticles for chemotherapy. Biomaterials 2000;21:1411–1420.
35. Margel S, Gura S. Nucleation and growth magnetic metal oxide nanoparticles. Natural and acquired antibodies. J Biomed Mater Res 2008;85:1011–1021.
36. Ziv O, Avtalion R, Margel S. Immunogenicity of bioactive magnetic nanoparticles: Natural and acquired antibodies. J Biomed Mater Res 2008;85:1011–1021.
37. Pankhurst QA, Connolly J, Jones SK, Dobson J. Applications of magnetic nanoparticles in biomedicine. J Phys D: App Phys 2003;36:167–181.
38. Peters T. All About Albumin: Biochemistry, Genetics and Medical Applications. San Diego, California: Academic Press; 1995. p 119.
39. Rozga M, Kloniecki M, Jablonowska A, Dadlez M, Bal W. The binding constant for amyloid Abeta40 peptide interactions with humen serum albumin. Biochem Biophys Res Commun 2007;364:714–718.
40. Tiruppahi C, Malik AB. Peptide carriers for drug delivery based on particular sequences of myeloperoxidase that serve as albumin docking proteins. Patent No. PTC/US2005/007442, 2007.
41. Berg W, Hillvarn B, Arwin H, Stenberg M, Lundstrom. The isoelecrtic point of thrombin and its behaviour compared to prothrombin at some solid surfaces. Thromb Haemost 1979; 42:972–982.
42. Horak D, Krystufek M, Spevacek J. Effect of reaction parameters on the dispersion polymerization of 1-vinyl-2-pyrrolidone. J Polym Sci A: Polym Chem 2000;38:653–663.
43. Bayele HK, Murdock PJ, Perry DJ, Pasi KJ. Simple shifts in redox/thiol balance that perturb blood coagulation. FEBS Lett 2002;510:67–70.